Thermal-Hydraulic Study of the DEMO Divertor Cassette Body Cooling Circuit Equipped with a Liner and Two Reflector Plates

P.A. Di Maio[a,*], G. Mazzone[b], A. Quartararo[a], E. Vallone[a], J.H. You[c]

[a]*Department of Engineering, University of Palermo, Viale delle Scienze, Ed. 6, 90128 Palermo, Italy*
[b]*Department of Fusion and Technology for Nuclear Safety and Security, ENEA C. R. Frascati, via E. Fermi 45, 00044 Frascati (Roma), Italy*
[c]*Max Planck Institute of Plasma Physics (E2M), Boltzmann Str.2, 85748 Garching, Germany*

Abstract

In the framework of the Work Package DIV 1 - "Divertor Cassette Design and Integration" of the EUROfusion action, a research campaign has been jointly carried out by University of Palermo and ENEA to investigate the steady-state thermal-hydraulic performances of the DEMO divertor cassette cooling system. The research activity has been focussed onto the most recent design of the Cassette Body (CB) cooling circuit, consistent with the DEMO baseline 2017 and equipped with a liner and two Reflector Plates (RPs), whose main functions are to protect the underlying vacuum pump hole from the radiation arising from plasma and shield the PFCs inlet distributors, respectively. The research campaign has been carried out following a theoretical-computational approach based on the finite volume method and adopting the commercial Computational Fluid-Dynamic (CFD) code ANSYS-CFX. The CB thermal-hydraulic performances have been assessed in terms of coolant and structure temperature, coolant overall total pressure drop and flow velocity distribution, mainly in order to check coolant aptitude to provide a uniform and effective cooling to CB, Liner and RPs structures. Moreover, the margin against coolant saturation has been evaluated in order check whether any risk of its bulk vaporisation is prevented. The outcomes of the study have shown some criticalities, mainly in terms of coolant bulk vaporization occurrence at the corner of the Inner Vertical Target (IVT) and uneven coolant flow distribution among RPs plasma-facing channels, that have suggested some design variations whose effectiveness has been numerically assessed. In particular, the solution proposed to contain and reduce the critical region of the IVT corner has been predicted to be particularly effective, while further studies are needed to improve coolant flow distribution among the RPs plasma-facing channels. Models, loads and boundary conditions assumed for the analyses are herewith reported and critically discussed, together with the main results obtained.

Keywords: DEMO, Divertor, Cassette Body, Thermofluid-dynamics, CFD analysis

1. Introduction

The European Research Roadmap to the Realisation of Fusion Energy has defined reliable power exhausting as one of the most critical missions. Heat-exhaust systems must handle the large heat and particle fluxes of a fusion power plant, allowing, at the same time, as high performance as possible from the core plasma [1].

The divertor is the key in-vessel component in this context, being responsible for power exhaust and impurity removal via guided plasma exhaust. As a consequence, the viability of fusion power generation heavily depends on the heat load that can be tolerated by the divertor under normal and off-normal operation [2]. Therefore, particular care has to be taken to design its cooling system, in order to ensure a uniform and proper cooling, without an unduly high pressure drop.

Within the framework of the Work Package DIV 1 - "Divertor Cassette Design and Integration" [3, 4] of the EUROfusion action and in line with previous activities [5, 6, 7, 8], a research campaign has been jointly carried out by University of Palermo and ENEA to assess the steady-state thermal-hydraulic performances of the DEMO divertor cassette cooling system.

During 2019, attention has been focussed on the assessment and optimisation of the thermal-hydraulic performances of the 2019 water-cooled CB design equipped with three shielding structures: a Liner and two Reflector Plates (RPs), to check whether the con-

sidered CB cooling circuits might provide a uniform and effective cooling of the steel structure, suitable to maintain its temperature under the prescribed limit of 550 °C [9], without incurring in coolant vaporization while minimizing the total pressure drop, thus the required pumping power.

Afterwards, on the basis of the issues arisen during this first thermal-hydraulic assessment, potential solutions devoted to its improvement have been investigated.

The research campaign has been performed following a theoretical-numerical approach based on the finite volume method and adopting the ANSYS CFX v.19.2 Computational Fluid-Dynamic (CFD) code [10], already used in similar studies [11] and adopted to evaluate concentrated hydraulic resistances to be used in system codes [12, 13]. The assumptions relevant to the thermal-hydraulic analyses are herein reported and critically discussed together with the main results obtained.

2. Outline of 2019 DEMO divertor cassette

DEMO divertor, according to its 2019 design [14], is articulated in 48 toroidal cassettes, each one composed of a Cassette Body (CB) equipped with a Liner and two RPs, and supporting two Plasma Facing Components (PFCs), namely Inner and Outer Vertical Target (IVT, OVT) (fig. 1). It differs from 2018 configuration for the revised CB shape, required to accommodate in-vessel coils at the inboard region and to embed the PFCs manifolds, and for the enhanced shielding ensured by the presence of the RPs, devoted to protecting the PFCs diffusers, and the thicker and larger Liner, which improves the neutron shielding for Vacuum Vessel and magnet coils.
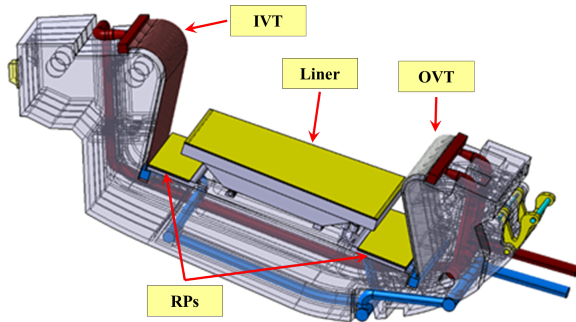

Figure 1: DEMO Divertor cassette (Design 2019).

During plant normal and off-normal operation, the CB will be subject to radiative heat fluxes and nuclear deposited heat power, requiring an active cooling that relies on the use of subcooled pressurized water at inlet pressure and temperature of 3.5 MPa and 180°C [14], respectively, flowing with a thermal rise of ≈30°C.

From the thermal-hydraulic standpoint, the CB acts as a coolant distributor/receiver for Liner and RPs, which are connected according to the scheme of fig. 2.
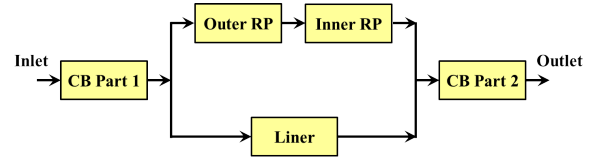

Figure 2: DEMO CB cooling scheme.

The Liner cooling circuit consists of four layers of cooling channels connected in series. The cooling water coming from the CB is routed, at first, to the Liner plasma-facing layer, composed of a parallel arrangement of 69 small circular cooling channels, then to the other three layers, cooled by quasi-rectangular large cooling channels, and in the end it is collected back to the CB. Concerning the RPs cooling circuit, it is composed of two layers of cooling channels connected in series. Inboard and outboard RPs plasma-facing layers are composed of a parallel arrangement of 109 and 87 circular cooling channels, respectively. The other layer is cooled by semi-circular large cooling channels both in case of inboard and outboard RP. The two RPs are connected to each other and to the CB cooling circuit by a set of four manifolds arranged in parallel.

3. CB cooling circuit CFD analysis

The thermal-hydraulic performances of the 2019 CB cooling circuit have been assessed by running a steady-state, thermally fully-coupled (fluid-structure) CFD analysis, according to the coolant operative conditions of table 1.

Table 1: Summary of coolant operative conditions.

	Operative Conditions
Inlet Pressure [MPa]	3.5
Inlet Temperature [°C]	180
ΔT [°C]	30
G per Cassette [kg/s]	31.17

The details of the mesh set up for the CFD analysis are reported in fig. 3 along with the main parameters in table 2. Assumptions, models and BCs adopted are summarised in table 3.

It is worth highlighting that the adopted meshing strategy and numerical modelling have been chosen on the basis of previous validation and mesh sensitivity analyses, and it has been selected in order to guarantee a good compromise between solution accuracy and computational costs.

Table 2: Summary of the main mesh parameters.

Region	Mesh Parameter	Value
	Nodes	$2.95 \cdot 10^7$
	Elements	$6.94 \cdot 10^7$
	Inflation Layers Number	12
	Liner/RPs First Cell Height [μm]	20
Fluid	Liner/RPs Layers Growth Rate	1.312
	CB First Cell Height [μm]	200
	CB Layers Growth Rate	1.400
	Typical Element Size [m]	$5.64 \cdot 10^{-3}$
	Surface with y^+<200 [%]	90.1
	Nodes	$5.60 \cdot 10^6$
Structure	Elements	$2.53 \cdot 10^7$
	Typical Element Size [m]	$6.71 \cdot 10^{-3}$

Table 3: Summary of assumptions, models and BCs.

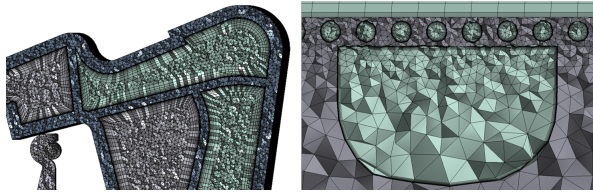| Analysis Type	Steady-state
	Water IAPWS IF97 [15]
	EUROFER [16]
Material Library	W / Ti6Al4V [17]
	316L(N) SS / SS 660 [17]
Liner / RPs Heat Flux	1.0 / 0.5 MW/m^2
Nuclear Heating	Non uniform
Radiative Heat Transfer	Towards VV @ 40°C
Turbulence Model	k-ϵ
Boundary Layer Modelling	Scalable Wall Functions
Wall Roughness	15 μm
Inlet BC	T=180°C / p_s=3.5 MPa
Outlet BC	G=31.17 kg/s

Figure 3: Mesh adopted for CB cooling circuit CFD analysis.

Concerning the considered heat loads, the non-uniform volumetric nuclear deposited power distribution calculated by ENEA Frascati Neutronics Team for the 2019 CB design [18] has been adopted (fig. 4). The detailed breakdown of the total deposited power, including both volumetric and surface heat loads is reported in table 4.

Furthermore, in order to properly take into account the presence of the vacuum vessel that, according to [19], is supposed to operate at 40 °C, a radiative heat transfer condition has been properly implemented in the CFD model.
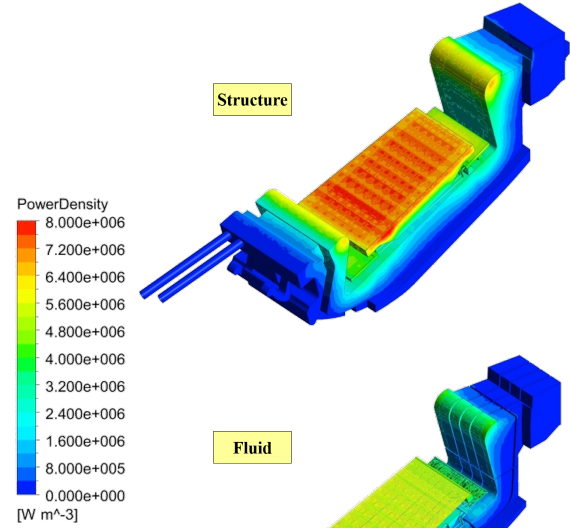

Figure 4: Nuclear heating distribution adopted for calculations.

Table 4: Deposited power breakdown for each Cassette.

Volumetric Heat Loads	
Component	Power [MW]
Liner Armour	0.084
Liner Structure	0.782
Liner Coolant	0.371
RPs Armour	0.024
RPs Structure	0.091
RPs Coolant	0.030
CB Structure	0.780
CB Coolant	0.376
TOTAL	2.538
Surface Heat Loads	
Component	Power [MW]
Liner Surface	1.511
RPs Surface	0.123
TOTAL	1.634

3

3.1. Results

The thermal-hydraulic performances of the CB cooling circuit under the nominal operative conditions of table 1 have been assessed mainly in terms of:

- coolant total pressure and total pressure drop distributions;

- mass flow rate branching between Liner and RPs,

- coolant flow velocity distribution among Liner and RPs plasma-facing channels;

- coolant temperature and sub-cooling margin distributions;

- coolant bulk temperature distribution among Liner and RPs channels;

- CHF margin distribution among Liner and RPs plasma-facing channels;

- structure temperature field.

The main obtained results are herein reported. In particular, coolant pressure distribution and total pressure drops between the main sections of the CB cooling circuit (fig. 5) are shown in fig. 6 and table 5, respectively.

Figure 6: CB coolant total pressure field.

Table 5: Coolant total pressure drop distribution.

Pressure Points	Δp [MPa]
Inlet → CB - A	0.0421
CB - A → Liner Inlet	0.0317
Liner Inlet → Liner Outlet (Liner)	0.6411
Liner Outlet → CB - B	0.0321
CB - A → RPs Inlet	0.0763
RPs Inlet → RPs A (Outer RP)	0.1506
RPs A → RPs B	0.2309
RPs B → RPs Outlet (Inner RP)	0.1611
RPs Outlet → CB - B	0.0859
CB - B → Outlet	0.0983
Cassette Total	**0.8452**

is caused by the much higher hydraulic resistance of the RPs cooling circuit if compared to the one of the Liner, mainly due to the manifold connecting the Outer to the Inner RP. In fact, since Liner and RPs cooling circuit are fed in parallel, the coolant mass flow rate fed to each one of them depends on the hydraulic resistance of the other one.

Moreover, coolant axial velocity distributions among Liner and RPs plasma-facing channels (fig. 7) are shown in fig. 8 and 9, summarising their key-parameters in table 7.

From the analysis of the results obtained, it may be argued that within the Liner plasma-facing channels the distribution of coolant axial flow velocity is acceptably uniform, since a maximum deviation of ≈3% has been estimated between the maximum (V_{Max}) and minimum
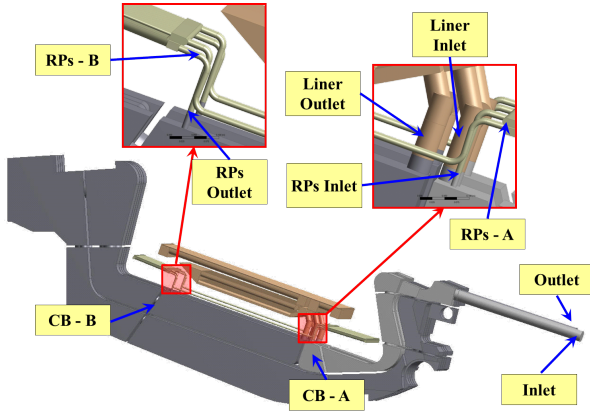

Figure 5: CB cooling circuit main sections.

Additionally, the calculated mass flow rate branching between Liner and RPs cooling circuit is reported in Table 6.

As it may be argued from the obtained results, the CB cooling circuit overall total pressure drop amounts to ≈0.85 MPa, being significantly lower than the prescribed limit of 1.4 MPa [14] and it is mainly concentrated within the Liner/RPs cooling circuits, as it may be expected. Moreover, most of the coolant mass flow rate is fed to the Liner (≈84%), while the remaining part (≈16%) is fed to the series connection of the RPs. This
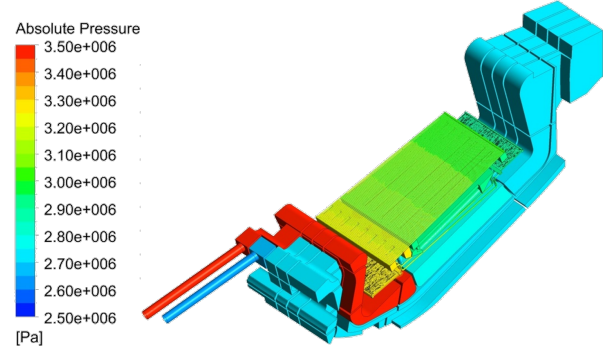
Table 6: CB cooling circuit mass flow rate distribution.

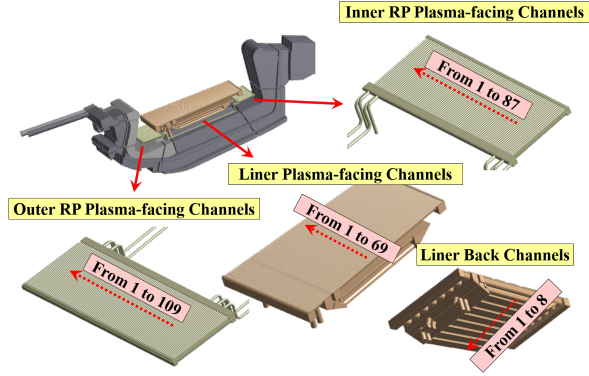| Sections	G [kg/s]	G/G_{tot}
Liner	26.25	84.2%
RPs	4.92	15.8%
Total	31.17	-

4

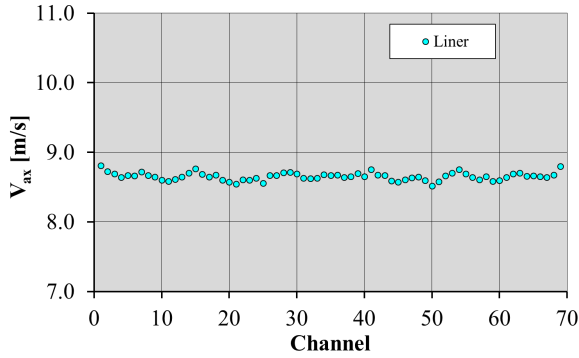Figure 7: Liner and RPs cooling circuit channels nomenclature.

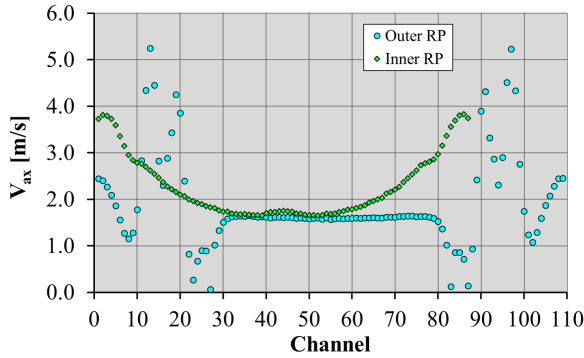Figure 8: Coolant axial flow velocity distribution among Liner front channels.

Figure 9: Coolant axial flow velocity distribution among RPs front channels.

Table 7: Coolant axial flow velocity distribution among Liner and RPs front channels key-parameters.

	Liner	Outer RP	Inner RP
V_{Max} [m/s]	8.807	5.250	3.831
V_{min} [m/s]	8.516	0.064	1.648
ϵ_V [%]	3.30	98.79	56.98
<V> [m/s]	8.654	1.906	2.290
Std. Deviation [m/s]	0.056	1.009	0.692

maximum and minimum values calculated as to Outer and Inner RP, respectively. As a consequence, the standard deviations calculated for both the two axial flow velocity distributions results to be significantly high.

In order to check whether these unbalanced coolant flow distributions might cause an uneven coolant temperature distribution that could eventually result in excessive thermal stresses in the steel structural components thus jeopardizing their integrity, attention has been focused on the coolant temperature distribution with particular reference to those locations where local coolant vaporisation might occur, hence compromising coolant heat transfer capabilities.

Therefore, coolant temperature distribution has been reported in fig. 10, while coolant margin against saturation, defined as $T_{sat}(p)$-T with $T_{sat}(p)$ drawn from [20], is shown in fig. 11, in which those areas where vaporization is predicted to occur have been reported in grey, while coloured zones represents those regions of the fluid domain where a positive margin against saturation is calculated.
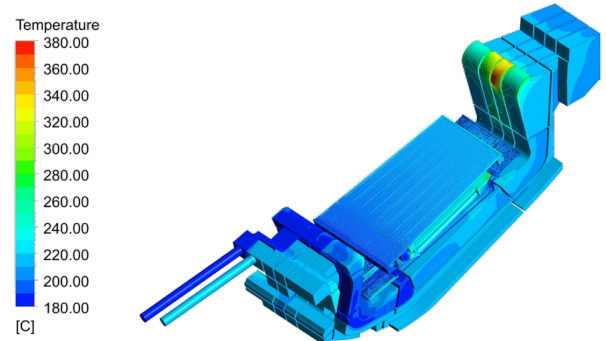

Figure 10: CB coolant temperature field.

(V$_{min}$) values. As a further confirmation, the standard deviation calculated for the axial flow velocity distribution amounts to 0.056 m/s, resulting quite low. On the contrary, the distributions of coolant axial flow velocity within the plasma-facing channels of both the two RPs are strongly uneven since maximum deviations in the order of 99% and 57% have been estimated between the

As it may be argued from the obtained results, the CB cooling circuit experiences wide coolant vaporisation within the IVT corner, the liner back channels headers and the CB outlet section. In particular, as coolant vaporisation extends to the bulk of the fluid, significant concerns arise from the IVT corner, being mainly due to its particular shape needed to accommodate the IVT
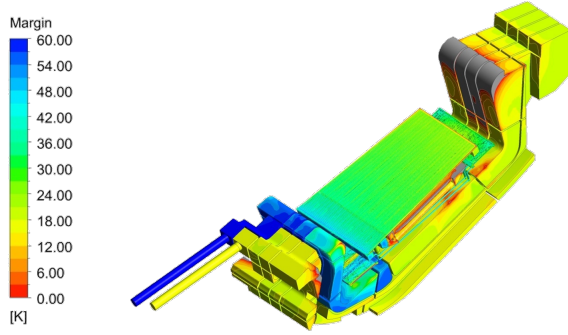
5

Figure 11: CB coolant margin against saturation field.

outlet header. Moreover, as it may be observed from the coolant flow streamlines in fig. 12, coolant is not properly conveyed towards the corner, being preferably directed to the outlet section of this box. It is worth notic-
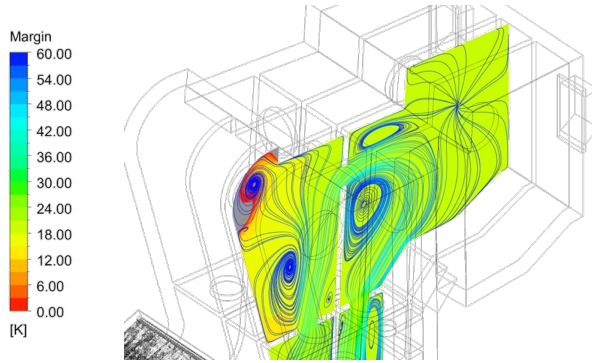

Figure 12: Detail of the CB coolant margin against saturation field at IVT corner.

ing how, as it may be observed in fig. 10, the coolant temperature distribution around the IVT corner shows a strong asymmetry, most likely due to a CB geometrical asymmetry, i.e. a restriction intended to accommodate the presence of the IVT outlet manifold. This asymmetry imprints a toroidal motion inside the CB, breaking the onset of a wider poloidal-radial vortex clearly visible in fig. 13. The development of this latter within the left box eases the coolant flowing towards the outlet section. This cannot happen within the right box, where the development of the poloidal-radial vortex is inhibited by the presence of the toroidal motion of the fluid. This vortex asymmetry affects significantly the local heat transfer coefficient, producing an hot spot inside the CB.

Therefore, in order to check whether these criticalities might extend to the bulk of the fluid, attention has been focussed on the coolant bulk temperatures at the
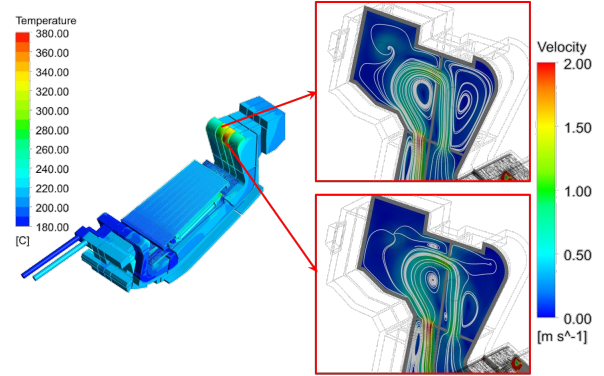

Figure 13: Flow velocity distributions at IVT corner poloidal-radial sections.

most relevant sections of the CB cooling circuit. In particular, coolant bulk temperatures and margins against saturation at the most relevant sections of the CB cooling circuit are synthetically reported in table 8.

Table 8: CB cooling circuit bulk temperature, saturation temperature and margin distributions.

Region	T_{bulk} [°C]	T_{sat} [°C]	Margin [°C]
Inlet	180.00	242.56	62.56
CB - A	182.98	241.87	58.89
Liner Inlet	183.33	241.34	58.01
Liner Outlet	206.80	229.77	22.97
RPs Inlet	183.24	240.59	57.35
RPs A	190.10	238.01	47.90
RPs B	190.15	233.86	43.71
RPs Outlet	195.28	230.82	35.54
CB - B	206.03	229.14	23.11
Outlet	210.03	227.17	17.15

Furthermore, the distributions of the margin against CHF onset within the Liner and RPs plasma-facing channels have been assessed adopting the correlation given in [21] and already employed in [22, 23, 24, 25], mainly in order to check whether its prescribed minimum value of 1.4 [14] is guaranteed by the present layout, and they have been reported in fig. 14 and 15 summarising their key-parameters in table 9.

Table 9: CHF margin distribution among Liner and RPs front channels key-parameters.

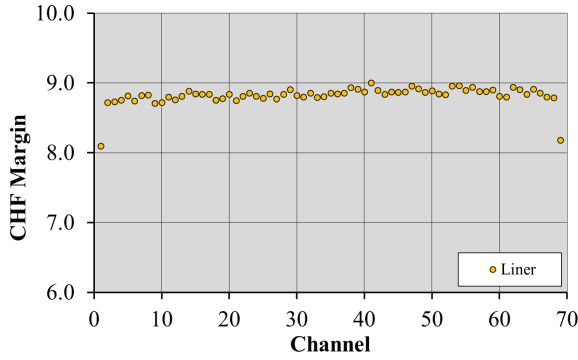|	Liner	Outer RP	Inner RP
(CHF Margin)$_{Max}$	9.000	41.239	33.113
(CHF Margin)$_{min}$	8.098	5.373	22.072
ϵ_{CHF} **[%]**	10.02	86.97	33.34
<CHF Margin>	8.823	24.137	24.771
Std. Deviation	0.135	5.603	3.130

6

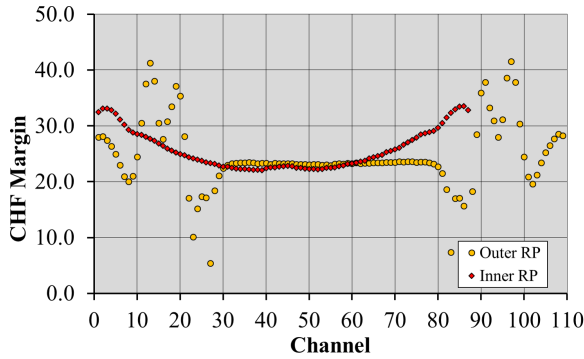Figure 14: CHF margin distribution among Liner front channels.

Figure 15: CHF margin distribution among RPs front channels.

From the analysis of the results obtained, it may be argued that the calculated distribution of CHF margin is acceptably uniform for the Liner plasma-facing channels, since a deviation between its maximum and minimum values amounts to ≈10%. Moreover, the values of CHF Margin calculated for the Liner channels result significantly higher than the prescribed limit of 1.4 in every single channel. On the other hand, the calculated distributions of CHF margin are strongly uneven for the RPs plasma-facing channels, since deviations between their pertaining maximum and minimum values amount to ≈87% and ≈33% as to Outer and Inner RP, respectively. Nevertheless, the values of CHF Margin calculated for RPs channels result significantly higher than the prescribed limit of 1.4 in every single channel. Finally, the structure temperature field has been reported in fig. 16 with a focus on the Eurofer working range that extends from 180 °C to 550 °C.

Results obtained have indicated that the CB cooling circuit seems to be able to provide a sufficiently uniform and effective cooling to the main part of the cassette steel structure. In fact, even if the peculiar structure of the Liner/RPs supports has always been somewhat crit-
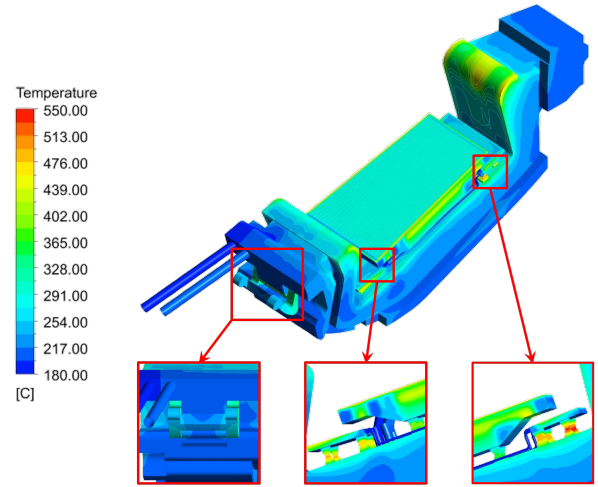

Figure 16: CB structure temperature field.

ical as it does not allow them to be properly cooled, the maximum temperature has been detected within the inner RP support system and amounts to 552.35 °C, only slightly higher than the limit of 550 °C. This result encourage a further design revision mainly intended to reduce the volume and, consequently, the thickness of the RPs supports and/or increase the shielding performance of the RPs nearby the support zones.

4. Revised CB Cooling Circuit CFD Analysis

As a consequence of the issues previously highlighted, in order to improve the velocity distributions among RPs plasma-facing channels, raise the minimum margin against saturation and prevent the occurrence of a wide coolant bulk vaporization, a revised layout of the CB cooling circuit has been issued. In particular, the following design changes have been implemented:

- RPs feeding manifolds layout revision and diameter increase from 12 mm to 15 mm (fig. 17);

- Inner RP plasma-facing channels diameter increase from 6 mm to 12 mm, while decreasing their overall number from 87 to 49 (fig. 17);

- Outer RP plasma-facing channels diameter increase from 6 mm to 12 mm, while decreasing their overall number from 109 to 62 (fig. 17);

- Liner plasma-facing channels diameter increase from 8 mm to 12 mm, while decreasing their overall number from 69 to 52 (fig. 17);

- originally missing connections introduction within the cassette outlet region where a wide coolant va-

porisation has been predicted to occur (in red in fig. 18);

- connections between boxes around the IVT corner rearranged (fig. 18);

- baffle plate introduction that might effectively route coolant flow towards the IVT corner (fig. 18).
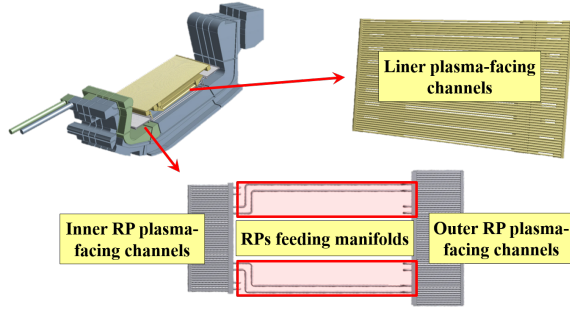

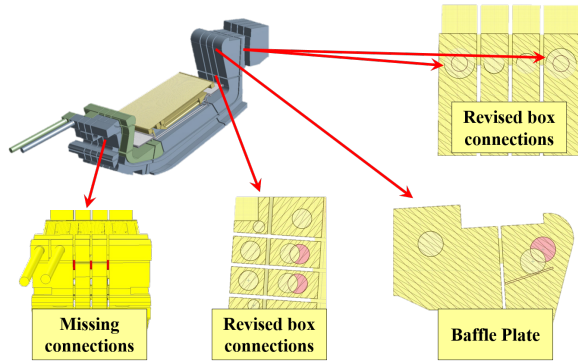Figure 17: Liner and RPs cooling circuits design revision.

Figure 18: CB cooling circuit design revision.

The thermal-hydraulic behaviour of the revised CB cooling circuit has been assessed assuming the coolant operative conditions of table 1.

4.1. Results

The results obtained for the revised CB cooling circuit CFD analysis in terms of coolant total pressure and total pressure drop distributions, mass flow rate distribution, coolant flow velocity distributions among Liner and RPs channels, coolant temperature and sub-cooling margin distributions, coolant bulk temperature and CHF margin distributions among Liner and RPs channels as well as structure temperature distribution are herein reported. The discretisation adopted together with loads

and boundary conditions selected have not been reported as they are the same of those shown in table 2 and 3, respectively.

In particular, coolant total pressure distribution and total pressure drops between the main sections of the CB cooling circuit (fig. 5) are shown in fig. 19 and table 10, respectively.
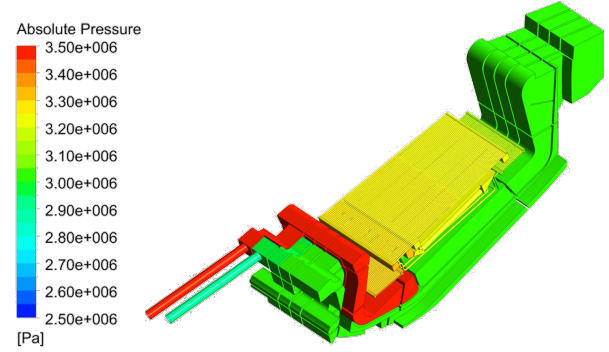

Figure 19: CB coolant total pressure field.

Table 10: Coolant total pressure drop distribution.

Pressure Points	Δp [MPa]
Inlet $\rightarrow$ CB - A	0.0420
CB - A $\rightarrow$ Liner Inlet	0.0296
Liner Inlet $\rightarrow$ Liner Outlet (Liner)	0.3568
Liner Outlet $\rightarrow$ CB - B	0.0305
CB - A $\rightarrow$ RPs Inlet	0.0413
RPs Inlet $\rightarrow$ RPs A (Outer RP)	0.1129
RPs A $\rightarrow$ RPs B	0.1276
RPs B $\rightarrow$ RPs Outlet (Inner RP)	0.0868
RPs Outlet $\rightarrow$ CB - B	0.0483
CB - B $\rightarrow$ Outlet	0.0985
Cassette Total	**0.5573**

As it may be argued from the obtained results, the revised CB cooling circuit overall total pressure drop amounts to ≈0.56 MPa with a reduction of ≈0.29 MPa (≈34%), if compared to the original design, being decreased the contribution of Liner/RPs cooling circuits to the overall total pressure drop. Moreover, coolant mass flow rate fed to the RPs cooling circuit has increased from 4.9 to 5.8 kg/s, amounting to ≈19% of the total mass flow rate fed to the CB cooling circuit. This is caused by the much lower hydraulic resistance of the RPs cooling circuit if compared to its original design, mainly due to the design revision of the manifold connecting the Outer to the Inner RP, whose percentage contribution is now comparable to those of the two RPs.

Moreover, coolant axial velocity distributions among Liner and RPs plasma-facing channels are shown in

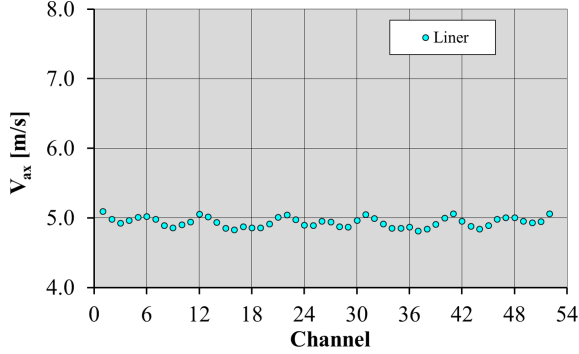fig. 20 and 21, summarising their key-parameters in table 11.

Figure 20: Coolant axial flow velocity distribution among Liner front channels.
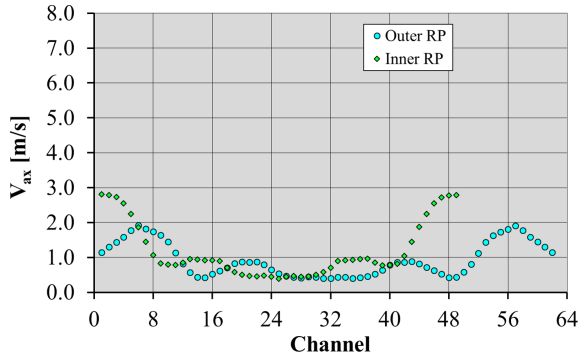

Figure 21: Coolant axial flow velocity distribution among RPs front channels.

Table 11: Coolant axial flow velocity distribution among Liner and RPs front channels key-parameters.

	Liner	Outer RP	Inner RP
V_{Max} [m/s]	5.095	1.923	2.806
V_{min} [m/s]	4.815	0.401	0.393
ϵ_V [%]	5.48	79.14	86.01
<V> [m/s]	4.939	0.936	1.192
Std. Deviation [m/s]	0.072	0.497	0.802

From the analysis of the results obtained, it may be argued that within the Liner plasma-facing channels the distribution of coolant axial flow velocity is acceptably uniform, since a maximum deviation of ≈5% has been estimated between the maximum and minimum velocity values. As a further confirmation, the standard deviation results to be quite low. On the contrary, both the two RPs still present strongly uneven distributions of coolant axial flow velocity within the plasma-facing

channels. In fact, even if the Outer RP coolant axial flow velocity distribution has been slightly flattened, the distribution calculated for the Inner RP is more uneven of the one pertaining to the original design, posing the need for a much deeper design change that might allow the coolant flow to get mixed within each RP header before being distributed to the RP channels.

Concerning the distributions of temperature and margin against saturation, these are reported in fig. 22 and 23, respectively, and summarized in table 12.
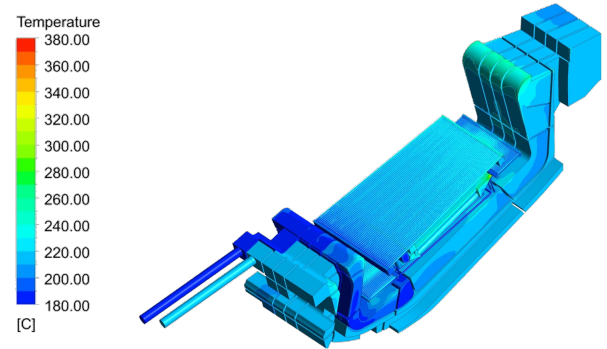

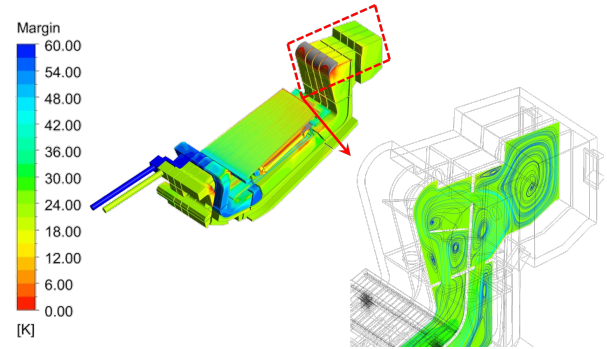Figure 22: CB coolant temperature field.

Figure 23: CB coolant margin against saturation field.

As it may be argued from the obtained results, no coolant bulk vaporisation has been predicted to occur within the revised CB cooling circuit. In this respect, the solution proposed to contain and reduce the critical region of the IVT corner has been predicted to be particularly effective. In fact, directing the coolant flow towards the corner, it makes indeed significantly uniform the distribution of the coolant margin against saturation around the corner, preventing coolant bulk vaporisation. Nevertheless, there are still extended critical zones at the fluid-structure interface to be further investigated, where a negative margin has been predicted.

Table 12: CB cooling circuit bulk temperature, saturation temperature and margin distributions.

Region	T_{bulk} [°C]	T_{sat} [°C]	Margin [°C]
Inlet	180.00	242.56	62.56
CB - A	182.97	241.87	58.90
Liner Inlet	183.28	241.38	58.09
Liner Outlet	207.66	235.17	27.51
RPs Inlet	183.44	241.18	57.74
RPs A	189.20	239.27	50.07
RPs B	189.35	237.04	47.70
RPs Outlet	193.63	235.49	41.86
CB - B	206.06	234.61	28.56
Outlet	210.31	232.79	22.48

Table 13: CHF margin distribution among Liner and RPs front channels key-parameters.

	Liner	Outer RP	Inner RP
(CHF Margin)$_{Max}$	6.458	21.92	25.180
(CHF Margin)$_{min}$	6.002	10.531	10.096
ϵ_{CHF} **[%]**	7.07	51.98	59.90
<CHF Margin>	6.307	15.063	15.999
Std. Deviation	0.077	3.770	4.884

Furthermore, the distributions of the margin against CHF onset within the Liner and RPs plasma-facing channels have been reported in fig. 24 and 25, summarising their key-parameters in table 13.
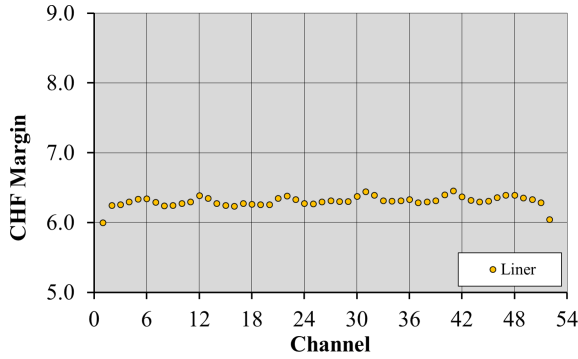

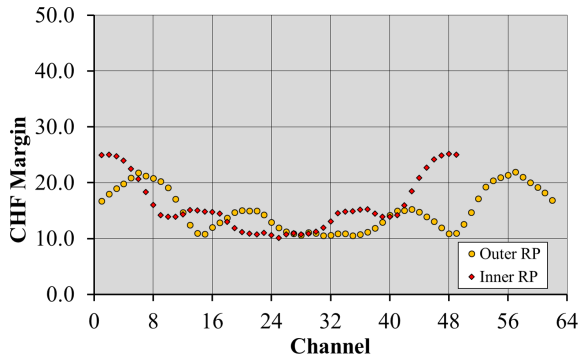Figure 24: CHF margin distribution among Liner front channels.

Figure 25: CHF margin distribution among RPs front channels.

From the analysis of the results obtained, it may be argued that the calculated distribution of CHF margin is acceptably uniform for the Liner plasma-facing channels, resulting significantly higher than the prescribed limit of 1.4 in every single channel. On the other hand, the calculated distributions of CHF margin are still strongly uneven for the RPs plasma-facing channels. Nevertheless, the values of saturation margin calculated for RPs channels result significantly higher than the prescribed limit in every single channel.

Concerning the structure temperature field, the results are not reported, since they are similar to those obtained for the original design and reported in fig. 16. In this regard, the maximum temperature has been located within the inner RP support system and amounts to 554.91 °C, only slightly higher than the one previously calculated.

This result encourage a further design revision mainly intended to reduce the volume and, consequently, the thickness of the RPs supports and/or increase the shielding performance of the RPs nearby the support zones.

5. Conclusions

Within the framework of the activities promoted by the EUROfusion consortium, a research campaign has been carried out by University of Palermo and ENEA to study the thermal-hydraulic behaviour of DEMO divertor cassette cooling system, focussing the attention on the CB cooling circuit 2019 configuration. A theoretical-computational approach based on the finite volume method has been followed and the ANSYS CFX code has been adopted.

The CB thermal-hydraulic performances have been assessed in terms of coolant and structure temperature, coolant overall total pressure drop and flow velocity distribution, mainly in order to check coolant aptitude to provide a uniform and effective cooling to CB, Liner and RPs structures. Moreover, the margin against coolant saturation has been evaluated in order check whether any risk of its bulk vaporisation is prevented.

The results obtained have highlighted the potential occurrence of coolant bulk vaporization, therefore, a revised layout of the CB cooling circuit has been issued. This latter configuration has demonstrated to be particularly effective in improving coolant temperature distribution at most of the critical locations previously iden-

tified. In particular, no coolant bulk vaporisation has been predicted to occur within the revised CB cooling circuit. Nevertheless, there are still unsolved issues to be properly addressed, mainly regarding the potential occurrence of a wide coolant vaporization at the fluid-structure interface. Therefore, in the next future, efforts are going to be primarily devoted to improve cooling to those regions where coolant stagnation is predicted to occur.

CRediT authorship contribution statement

P.A. Di Maio: Conceptualization, Methodology, Investigation, Writing - original draft. **J.H. You**: Conceptualization, Methodology, Investigation, Writing - original draft. **G. Mazzone**: Conceptualization, Methodology, Investigation, Writing - original draft. **A. Quartararo**: Conceptualization, Methodology, Investigation, Writing - original draft. **E. Vallone**: Conceptualization, Methodology, Investigation, Writing - original draft.

Declaration of Competing Interest

The authors declare that they have no known competing financial interests or personal relationships that could have appeared to influence the work reported in this paper.

Acknowledgments

References

[1] T. Donné, W. Morris, European Research Roadmap to the Realisation of Fusion Energy, 2018, ISBN: 978-3-00-061152-0.

[2] G. Federici, et al., Overview of the DEMO staged design approach in Europe, Nuclear Fusion 59 (2019) 066013. `doi:10.1088/1741-4326/ab1178`.

[3] J.H.You, et al., Conceptual design studies for the European DEMO divertor: Rationale and first results, Fusion Engineering and Design 109–111 (2016) 1598–1603. `doi:10.1016/j.fusengdes.2015.11.012`.

[4] J.H.You, et al., Progress in the initial design activities for the European DEMO divertor: Subproject "Cassette", Fusion Engineering and Design 124 (2017) 364–370. `doi:10.1016/j.fusengdes.2017.03.018`.

[5] P.A. Di Maio, et al., Analysis of steady state thermal-hydraulic behaviour of the DEMO divertor cassette body cooling circuit, Fusion Engineering and Design 124 (2017) 437–441. `doi:10.1016/j.fusengdes.2017.02.012`.

[6] P.A. Di Maio, et al., Computational thermofluid-dynamic analysis of DEMO divertor cassette body cooling circuit, Fusion Engineering and Design 136 (2018) 1588–1592. `doi:10.1016/j.fusengdes.2018.05.063`.

[7] P.A. Di Maio, et al., Thermal-hydraulic optimisation of the DEMO divertor cassette body cooling circuit equipped with a liner, Fusion Engineering and Design 146 (2019) 220–223. `doi:10.1016/j.fusengdes.2018.12.024`.

[8] P.A. Di Maio, et al., On the thermal-hydraulic performances of the DEMO divertor cassette body cooling circuit equipped with a liner, Fusion Engineering and Design 156 (2020) 111613. `doi:10.1016/j.fusengdes.2020.111613`.

[9] B. van der Schaaf, et al., The development of EUROFER reduced activation steel, Fusion Engineering and Design 69 (2003) 197–203. `doi:10.1016/S0920-3796(03)00337-5`.

[10] ANSYS Inc., ANSYS CFX-Solver Theory Guide, 2019, Release: 2019 R1.

[11] P.A. Di Maio, et al., On the hydraulic behaviour of ITER Shield Blocks #14 and #08. Computational analysis and comparison with experimental tests, Fusion Engineering and Design 109-111 (2016) 30–36. `doi:10.1016/j.fusengdes.2016.03.060`.

[12] P.A. Di Maio, et al., Analysis of the steady state hydraulic behaviour of the ITER blanket cooling system, Fusion Engineering and Design 98-99 (2015) 1470–1473. `doi:10.1016/j.fusengdes.2015.05.070`.

[13] P.A. Di Maio, et al., Numerical simulation of the transient thermal-hydraulic behaviour of the ITER blanket cooling system under the draining operational procedure, Fusion Engineering and Design 98-99 (2015) 1664–1667. `doi:10.1016/j.fusengdes.2015.01.024`.

[14] G. Mazzone, et al., Eurofusion-DEMO Divertor - Cassette Design and Integration, Fusion Engineering and Design 157 (2020) 111656. `doi:10.1016/j.fusengdes.2020.111656`.

[15] International Association for the Properties of Water and Steam, Revised Release on the IAPWS Industrial Formulation 1997 for the Thermodynamic Properties of Water and Steam, 2007.

[16] F. Gillemot and et al., Material Property Handbook pilot project on EUROFER97 (MTA EK, KIT), 2016, EUROfusion IDM Ref.: 2MRP77.

[17] ITER Material Properties Handbook, ITER Document No. G74 MA 16.

[18] R. Villari, et al., Neutronics studies in support of European DEMO Divertor design, this conference.

[19] T. Haertl, et al., Rationale for the selection of the operating temperature of the DEMO vacuum vessel, Fusion Engineering and Design 146 (2019) 1096–1099. `doi:10.1016/j.fusengdes.2019.02.014`.

[20] P.J. Linstrom, W.G. Mallard, Eds., NIST Chemistry WebBook, NIST Standard Reference Database Number 69 ,National Institute of Standards and Technology, Gaithersburg MD, 20899 (retrieved September 9, 2019). `doi:10.18434/T4D303`.

[21] A.R. Raffray, et al., Critical heat flux analysis and R&D for the design of the ITER divertor, Fusion Engineering and Design 45 (4) (1999) 377–407. `doi:10.1016/S0920-3796(99)00053-8`.

[22] P.A. Di Maio, et al., Thermal-hydraulic behaviour of the DEMO divertor plasma facing components cooling circuit, Fusion Engineering and Design 124 (2017) 415–419. `doi:10.1016/j.fusengdes.2017.02.025`.

[23] P.A. Di Maio, et al., On the thermal-hydraulic optimization of

DEMO divertor plasma facing components cooling circuit, Fusion Engineering and Design 136 (2018) 1438–1443. `doi:10.1016/j.fusengdes.2018.05.032`.

[24] P.A. Di Maio, et al., Hydraulic analysis of EU-DEMO divertor plasma facing components cooling circuit under nominal operating scenarios, Fusion Engineering and Design 146 (2019) 1764–1768. `doi:10.1016/j.fusengdes.2019.03.030`.

[25] P.A. Di Maio, et al., On the numerical assessment of the thermal-hydraulic operating map of the DEMO Divertor Plasma Facing Components cooling circuit, Fusion Engineering and Design 161 (2020). `doi:10.1016/j.fusengdes.2020.111919`.